Optical Investigation of Nd^{3+}-sensitized Upconversion Nanoparticles for Damage-free *in vivo* Deep Imaging and *in vitro* Microscopy

Yuxiang Zhao and Qiuqiang Zhan*
Centre for Optical and Electromagnetic Research, South China Academy of Advanced Optoelectronics
South China Normal University (SCNU), Guangzhou 510006, China

Abstract— We firstly set up two optical models and investigated the upconverting excitation process of novel 795-nm excited Nd^{3+}-sensitized upconversion nanoparticles. Simulation results proved the novel UCNPs has the potential to show excellent *in vivo* deep imaging and damage-free *in vivo*, *in vitro* imaging ability under high power 795 nm laser excitation.

1. INTRODUCTION

Upconversion nanoparticles (UCNPs) have been demonstrated as the hot nanoprobes in the biophotonics research [1]. Superior to the conventional biological labels such as organic dyes and quantum dots UCNPs exhibit the unique properties of autofluorescence-free bioimaging under near-infrared light excitation Due to series of advantages such as large anti-Stokes shifts no photobleaching, no blinking, low cytotoxicity, deep imaging ability and high resolution UCNPs have attracted huge attention and interests in the biomedical and biotherapy in recent years [2]. However, traditional Yb^{3+}-sensitized UCNPs have been proved to reduce the overheating effect under high power 975 nm laser excitation [3]. Recently, Nd^{3+}-sensitized UCNPs have emerged as a candidate to replace traditional ones due to the minimized heating effect under 795 nm laser excitation [4]. Some groups have presented the synthesis and potential applications of Nd^{3+}-sensitized UCNPs which were still lack of optical investigation [5–7]. In this work, we optically modeled for Nd^{3+}-sensitized UCNPs-based bio-applications and showed the damage-free imaging ability using 795 nm laser exciting. Meanwhile, the Nd^{3+} to Yb^{3+} energy transfer efficiency was discussed to study the impact on deep imaging ability.

2. MODELING AND THEORETICAL METHODS

2.1. Optical Models

Two different optical models of UCNPs-based biomedical applications were constructed to investigate the Nd^{3+}-sensitized UCNPs: one is a cell-in-celldish model for *in vitro* microscopy; the other is a pork tissue model for *in vivo* deep tissue imaging.

2.1.1. Cell-in-celldish Model

As shown in Fig. 1(a) a cylinder area (diameter: 35 mm depth: 3 mm) was set up as PBS solution in cell-in-celldish for the investigation of *in vitro* microscopy while the UCNPs-labeled cells were adherent on the bottom. We simulated it on an inverted microscope with 100 mW high power CW laser exciting after focused by a 1.35 NA objective.

2.1.2. Pork Tissue Model

As described in Fig. 1(b), we selected the three layers (2.5 mm skin, 12.5 mm fat and 30 mm muscle) cylinder pork tissue model as its similar tissue optical properties with human beings, which acted as the part of tissue being irradiated by circle area (radius: 25 mm) CW laser source (power density: 500 mW/cm^2). A UCNPs-labeled tumor (radius: 2.5 mm) was in this tissue model at different depth from 5 mm to 42.5 mm.

2.2. Theoretical Methods

The theoretical methods of these two models are based on three different ones: diffusion equation heat transport equation and cell damage model, each of which is described as below and the parameters used are set as typical values [3, 8–13].

*Corresponding author: Qiuqiang Zhan (qiuqiang.zhan@coer-scnu.org).

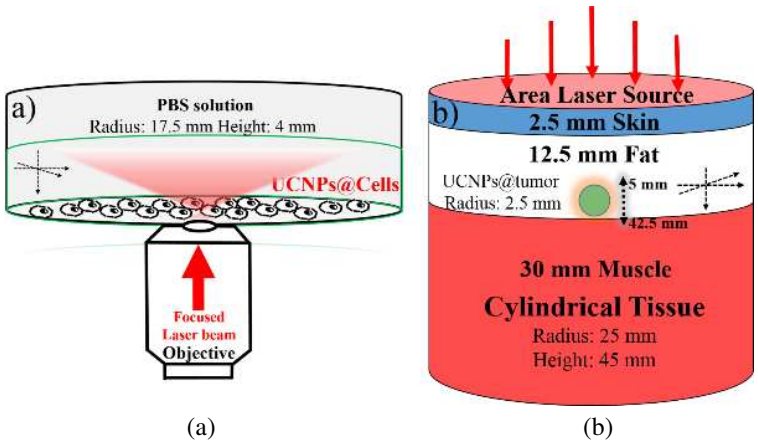

(a) (b)

Figure 1: Schematics of (a) *in vitro* cell-in-celldish model and (b) *in vivo* Pork Tissue model.

2.2.1. Diffusion Equation

Fluorescence diffusing imaging can be described as two equations: one is the excitation light Equation (1) and the other is the fluorescence emission Equation (2). In the steady state, we can describe them as [8]:

$$-\nabla(D_{ex}\nabla\varphi_{ex}) + \mu_a^{ex}\varphi_{ex}(r) = S(r) \tag{1}$$

$$-\nabla(D_{em}\nabla\varphi_{em}) + \mu_a^{em}\varphi_{em}(r) = \eta\mu_{ex}[\varphi_{ex}(r)]^2 \quad \text{for 975 nm laser} \tag{2a}$$

$$-\nabla(D_{em}\nabla\varphi_{em}) + \mu_a^{em}\varphi_{em}(r) = \eta\mu_{ex}[Y\varphi_{ex}(r)]^2 \quad \text{for 795 nm laser} \tag{2b}$$

where μ_a, μ_s', and $D_{ex/em} = 1/(3*(\mu_a^{ex/em} + \mu_s^{'ex/em}))$ denotes the absorption coefficient, reduced scattering coefficient and diffusion coefficient of excitation or emission light; Y is the energy transfer efficient from Nd^{3+} to Yb^{3+}, $\varphi_{ex/em}$ is the photon fluence rate of excitation and emission light and η is the power-related quantum yield coefficient of UCNPs For the side boundary and interface between 3 layers, we regard them as continuous conditions. Neumann boundary condition is used that accounts for the refractive index mismatch between tissue ($n_{tissue} \sim 1.4$) and air ($n_{air} \sim 1$) as: $n \cdot (D\nabla\varphi(r,t)) + \varphi(r,t)/2A = 0$, where A is 2.74 in this investigation.

2.2.2. Heat Transfer Equation

The spatiotemporal temperature distribution for two models are based on the Pennes' bioheat transfer equation with an additional term Q [14, 15]:

$$\rho c(dT/dt) = (kT) + Q \tag{3}$$

where the first term on the right side is heat conduction. The second term heat source Q absorbed can be obtained according to the lambert-Beer law for the *in vitro* model and calculated as $Q = \mu_a^{ex}\varphi_{ex}(r)$ from Equation (1) for the *in vivo* model. Regarding the boundary conditions, a heat flux condition was used combined with Newton's law of cooling to describe a convection process as: K $(\mathrm{d}T/\mathrm{d}n) = h(T - T_0)$ where $h_{air} = 25\,\mathrm{W/(m^2 \cdot K)}$, $h_{wall} = 5\,\mathrm{W/(m^2 \cdot K)}$

2.2.3. Cell/Tissue Damage Model

Here we predict this cell/tissue damage by using the Arrhenius injury model. The cells/tissue that are damaged over time is given by [12, 15]:

$$F_D = 1 - e^{-\Omega} = 1 - e^{-\int k dt} = 1 - e^{-\int Ae - Ea/(RT)dt} \tag{4}$$

where Ω is the damage index E_a is the activation energy, R is the universal gas constant, T is the temperature changed with time, and A is a scaling factor. Here we define healthy cell has $F_D = 0$, and $F_D = 0.6$ means the time cell begin to be damaged.

3. RESULTS AND DISCUSSION

3.1. Damage-free *in vitro* Microscopy with Nd^{3+}-sensitized UCNPs

In this simulation, 100 mW (focal plane power) CW laser beam was used [16]. In the *in vitro* microscopy, heating effect was primarily due to the absorption of exciting laser. As shown in Figs. 2(a)–(d), the spatiotemporal temperature distribution changed very little under 795 nm excitation, whereas under the 975 nm excitation the temperature had a huge raising after 20 minutes. After 30 s of irradiation, it didn't reach the apoptosis temperature under either 795 nm or 975 nm laser excitation. After 20 minutes-irradiation, the temperature increased to 46°C and most cells were damaged in the case of 975 nm laser in Fig. 2(h). On the contrary, almost all the cells were still healthy under high power 795 nm excitation after 20 minutes in Fig. 2(f), which was attributed to the minimized heating effect of Nd^{3+}-sensitized UCNPs.

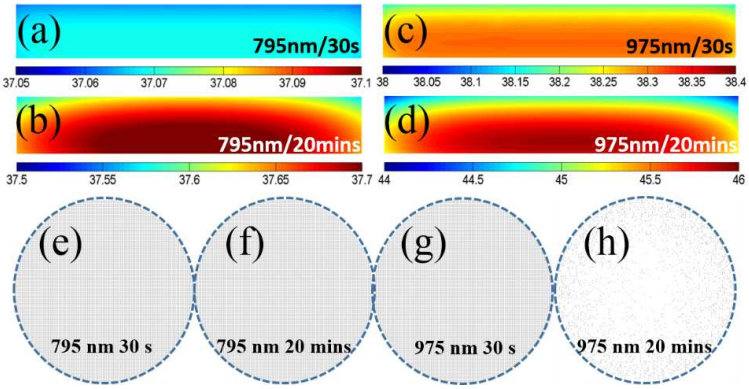

Figure 2: Simulated spatiotemporal temperature distributions of cell-in-celldish model under (a) 30 s, (b) 20 mins 795 nm laser excitation and (c) 30 s, (d) 10 mins 975 nm laser excitation (focal plane power: 100 mW). Cell viability predictions under (e) 1 min, (f) 20 mins 975 nm laser irradiation and (g) 1 min, (h) 20 mins 795 nm laser irradiation.

3.2. Damage-free *in vivo* Tissue Imaging with Nd^{3+}-sensitized UCNPs

500 mW/cm^2 circle area CW laser was selected in our simulation which had been proved to reduce the overheating effect in skin surface under 975 nm laser excitation [3]. Compared to the results in Fig. 3(a), each corresponding pictures in Fig. 3(b) showed a much higher temperature. After 3 minutes of 975 nm laser irradiation, temperature raised above 45°C and the inner part of skin was almost damaged in Fig. 3(e). After irradiated by high power 975 nm laser for 10 minutes, the damage condition in tissue was extremely severe as the temperature was up to 60°C. On the contrary, under high power 795 nm laser excitation the temperature had not reached 40°C and the

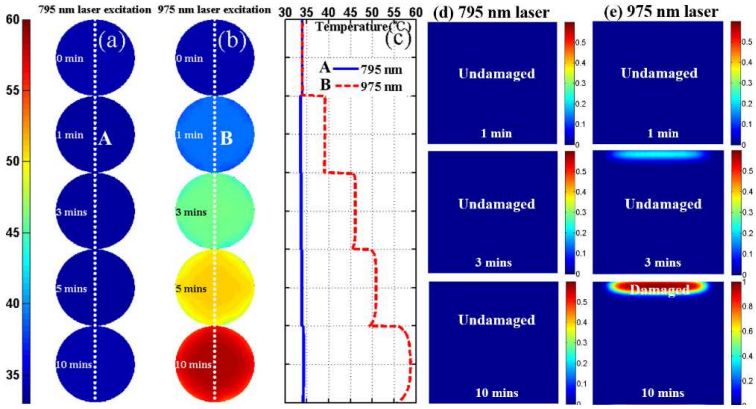

Figure 3: Simulated temperature distributions after different irradiation times of pork tissue model surface under (a) 795 nm, (b) 975 nm laser irradiation and (c) the corresponding temperature line. Simulated normalized tissue damage index distributions of pork tissue model after different time irradiation of (d) 795 nm and (e) 975 nm laser.

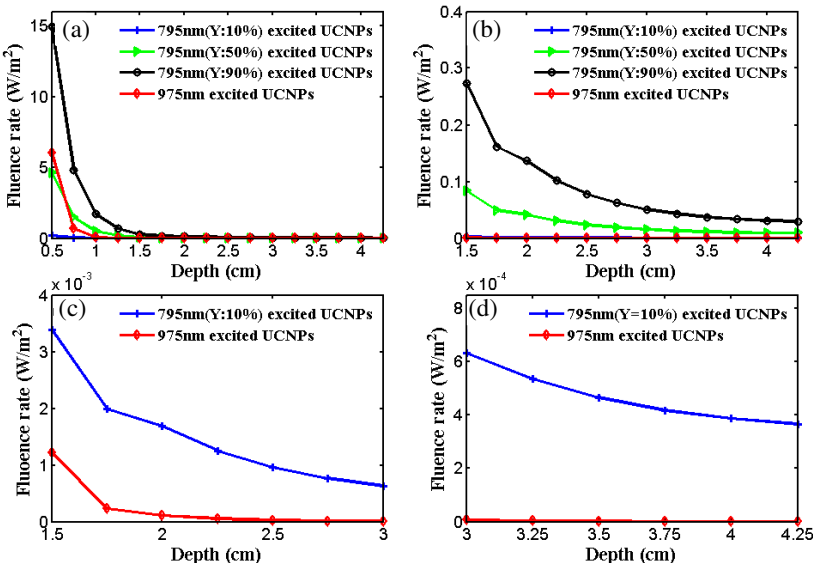

Figure 4: Stimulated UC PL fluence rate at detector point for different tumor depth (from 0.5 cm to 4.25 cm) of 500 mW/m^2 975 nm laser and 795 nm laser with different energy transfer efficient Y (10%, 50%, 90%) from $Nd^{3+}Yb^{3+}$.

whole tissue still kept undamaged even after 1 minutes of irradiation. Simulation results proved that the Nd^{3+}-sensitized UCNPs completely exhibit the damage-free *in vivo* deep imaging ability.

3.3. Nd^{3+} to Yb^{3+} Energy Transfer Efficiency (ETE) Dependent Deep *in vivo* Tissue Imaging

The upconversion (UC) photoluminescence (PL) process of Nd^{3+}-sensitized UCNPs is based on the energy transfer bridge Yb^{3+} (Nd^{3+}-Yb^{3+}-Ln^{3+}), which should be considered into deep tissue imaging application. In this simulation, 795-nm excited Nd^{3+}-sensitized UCNPs with 650 nm emission and 975 nm excited UCNPs with 800 nm emission were used to investigate the impact of ETE on the imaging depth. As shown in Fig. 4, the intensities of 800 nm UC emission (under 975 nm excitation) and 650 nm UC emission (under 795 nm excitation with different Y from 10% to 90%) on the surface were showed at different tumor depths from 0.5 cm to 4.25 cm. The surface UC PL intensity decreased rapidly with exciting depth increased because the much higher scattering and absorption in deep tissue. The 795 nm excited UCNPs ($Y \geq 50\%$) with 650 nm emission has a better deep (≥ 0.75 cm) imaging ability than 975-nm-excited ones. In the deep (≥ 1.5 cm) region showed in Figs. 4(d) and (e), Nd^{3+}-sensitized UCNPs ($Y = 10\%$) can replace the Yb^{3+}-sensitized ones which indicated the high deep imaging of the 795-nm-excited ones.

4. CONCLUSION

For the first time both *in vitro* cell microscopy and *in vivo* 3-layers pork tissue have been optically modeled systematically to give a new perspective to the study of Nd^{3+}-sensitized UCNPs. With two optical models, the spatiotemporal temperature and damage distribution have been investigated as the complementary research of Nd^{3+}-sensitized UCNPs. We have calculated and presented this novel UCNPs as the damage-free nanoprobes in both *in vitro* and *in vivo* imaging under high power laser irradiation by shifting the exciting wavelength from 975 nm to 795 nm. Simulation results of deep tissue imaging have exhibited the novel UCNPs with higher ($\geq 5\%$) Nd^{3+} to Yb^{3+} energy transfer efficiency are worth to be synthesized for *in vivo* deep tissue bio-applications.

ACKNOWLEDGMENT

This work was supported by Guangdong Innovative Research Team Program (No. 201001D01047993 18), the Natural Science Foundation of Guangdong province (No. S2013040014211), the Postdoctoral Science Foundation of China (No. 2013M530368), the Discipline and Specialty Construction Fundation of Colleges and Univerisities of Guangdong Province (No. 2013LYM_0017), the Young Faculty Academic Training Foundation of SCNU (No. 2012KJ017), and the Student Extracurricular Scientific Research Key Project of SCNU (No. 13GDKC02).

REFERENCES

1. Liu, Y., et al., "Lanthanide-doped luminescent nanoprobes: Controlled synthesis, optical spectroscopy, and bioapplications," *Chemical Society Reviews*, Vol. 16, 6924–6958, 2013.
2. Xu, C. T., et al., "Upconverting nanoparticles for pre-clinical diffuse optical imaging, microscopy and sensing: Current trends and future challenges," *Laser & Photonics Reviews*, Vol. 5, 663–697, 2013.
3. Zhan, Q., et al., "Using 915 nm laser excited $Tm^{3+}/Er^{3+}/Ho^{3+}$-doped NaYbF4 upconversion nanoparticles for in vitro and deeper in vivo bioimaging without overheating irradiation," *ACS Nano*, Vol. 5, 3744–3757, 2011.
4. Wang, Y.-F., et al., "Nd^{3+}-sensitized upconversion nanophosphors: Efficient in vivo bioimaging probes with minimized heating effect," *ACS Nano*, Vol. 8, 7200–7206, 2013.
5. Li, X., et al., "Nd^{3+} sensitized up/down converting dual-mode nanomaterials for efficient in-vitro and in-vivo bioimaging excited at 800 nm," *Sci. Rep.*, 2013.
6. Xie, X., et al., "Mechanistic investigation of photon upconversion in Nd^{3+}-sensitized core-shell nanoparticles," *Journal of the American Chemical Society*, Vol. 34, 12608–12611, 2013.
7. Zhong, Y., et al., "Elimination of photon quenching by a transition layer to fabricate a quenching-shield sandwich structure for 800 nm excited upconversion luminescence of Nd^{3+}-sensitized nanoparticles," *Advanced Materials*, Vol. n/a–n/a, 2013.
8. Xu, C. T., J. Axelsson, and S. Andersson-Engels, "Fluorescence diffuse optical tomography using upconverting nanoparticles," *Applied Physics Letters*, Vol. 25, 2009.
9. Zhan, Q., et al., "Optimization of optical excitation of upconversion nanoparticles for rapid microscopy and deeper tissue imaging with higher quantum yield," *Theranostics*, Vol. 5, 306, 2013.
10. George, A., R. R. Fernando, and F. C. Arion, "Tomographic bioluminescence imaging by use of a combined optical-PET (OPET) system: A computer simulation feasibility study," *Physics in Medicine and Biology*, Vol. 17, 4225, 2005.
11. Rylander, M. N., et al., "Optimizing heat shock protein expression induced by prostate cancer laser therapy through predictive computational models," *Journal of Biomedical Optics*, Vol. 4, 041113-041113–16, 2006.
12. Henriques, F. C., "Studies of thermal injury; the predictability and the significance of thermally induced rate processes leading to irreversible epidermal injury," *Archives of Pathology*, Vol. 5, 489–502, 1947.
13. Cohen, M. L., "Measurement of the thermal properties of human skin. A review," *Journal of Investigative Dermatology*, Vol. 3, 333–338, 1977.
14. Pennes, H. H., "Analysis of tissue and arterial blood temperatures in the resting human forearm," *Journal of Applied Physiology*, Vol. 2, 93–122, 1948.
15. Rylander, M. N., et al., "Heat shock protein expression and injury optimization for laser therapy design," *Lasers in Surgery and Medicine*, Vol. 9, 731–746, 2007.
16. Liu, Q., et al., "Upconversion luminescence imaging of cells and small animals," *Nat. Protocols*, Vol. 10, 2033–2044, 2013.